From colour fingerprinting to the control of photoluminescence in elastic photonic crystals

ANDRÉ C. ARSENAULT[1]*, TIMOTHY J. CLARK[1], GEORG VON FREYMANN[1,2]†, LUDOVICO CADEMARTIRI[1], RICCARDO SAPIENZA[3], JACOPO BERTOLOTTI[3], EVANGELLOS VEKRIS[1], SEAN WONG[1], VLADIMIR KITAEV[1‡], IAN MANNERS[1], R. Z. WANG[2], SAJEEV JOHN[2], DIEDERIK WIERSMA[3] AND GEOFFREY A. OZIN[1]*

[1]Department of Chemistry, University of Toronto, 80 St. George Street, Toronto M5S 3H6, Canada
[2]Department of Physics, University of Toronto, 60 St. George Street, Toronto M5S 1A7, Canada
[3]European Laboratory for Non-linear Spectroscopy and INFM-Matis, via Nello Carrara 1, 50019 Sesto Fiorentino, Firenze, Italy
†Present address: Institut für Nanotechnologie, Forschungszentrum Karlsruhe in der Helmholtz-Gemeinschaft, 76021 Karlsruhe, Germany
‡Present address: Department of Chemistry, Wilfred Laurier University, 75 University Avenue West, Waterloo N2L 3C5, Canada
*e-mail: aarsenau@chem.utoronto.ca; gozin@chem.utoronto.ca

In photonic crystals (PCs), strong scattering and destructive wave interference lead to a modification of the photon density of states in particular energy regions and along certain crystallographic directions[1,2]. The consequences of this range from suppression and enhancement of luminescence[3–7] to narrow-band bright reflections useful for colour sensors[8,9], displays[10] and tuneable filters[11–14]. Here we demonstrate large-area films of porous elastomeric photonic crystals (EPCs) that are compressively–decompressively cycled to reversibly shift the position of the photonic band structure over a large wavelength range. Owing to their low compressive threshold, such porous EPCs can be used for imaging that is pressure and time sensitive, for example, to obtain colour fingerprints with high accuracy. Furthermore, by incorporating luminescent PbS quantum dots in the EPCs, the photonic stop-gap can be tuned through the near-infrared (NIR) quantum dot photoluminescence (PL) peak. Thereby we demonstrate a tuneable modification of photonic characteristics, including the suppression and enhancement in emission and dynamic modification of luminescence lifetimes.

Since their inception[15,16], PCs have garnered ever-increasing scientific interest. Such synthetic materials have a periodic modulation in their refractive index and diffract light of wavelengths commensurate to their periodicity. Although only a fraction of PCs bear a full photonic bandgap[17,18], a range of energies where photons cannot propagate in any direction, all PCs have stop-gaps that forbid propagation in certain crystallographic directions. Within a photonic stop-gap, light emission can be markedly suppressed[3,4]. Light in this spectral range is also efficiently reflected. This is useful for sensors with a colour-based response if an analyte can modulate the refractive index or lattice spacing[8], or for colour display systems if such modulations can be effected by an electric or electrochemical stimulus[10]. At the photonic band edges, light propagates at reduced group velocities owing to resonant Bragg scattering, which can enhance luminescence owing to stimulated emission[5,6] and amplify the absorption of incident light to boost the efficiency of photovoltaic cells[19].

Given that PCs show such important optical effects, it is necessary to identify versatile materials that can accommodate diverse applications. A particularly desirable attribute is a reversible post-fabrication tunability. This would allow a particular PC to be reconfigured for different functions or to be continuously tuned, as would be required of a variable filter or laser source. Another important consideration is the ability to incorporate active species into this structure without degrading its structural and optical integrity. We demonstrate here an elastomer-based PC platform that is reversibly tunable and stable to extended cycling. The potential of this material is demonstrated by accurate, pressure-dependent colour fingerprinting, as well as by tuning the characteristics of spontaneous emission from encapsulated NIR-emitting quantum dots.

In this study, we used a templating strategy to fabricate the EPC materials, which gives us control over both the material composition and structural order. The method is summarized in Fig. 1 and begins with high-quality silica microsphere films on glass[20,21]. The films are filled with a mixture of monomer, crosslinking agent and photoinitiator, and are photopolymerized to generate an elastomeric network. The excess polymer is then
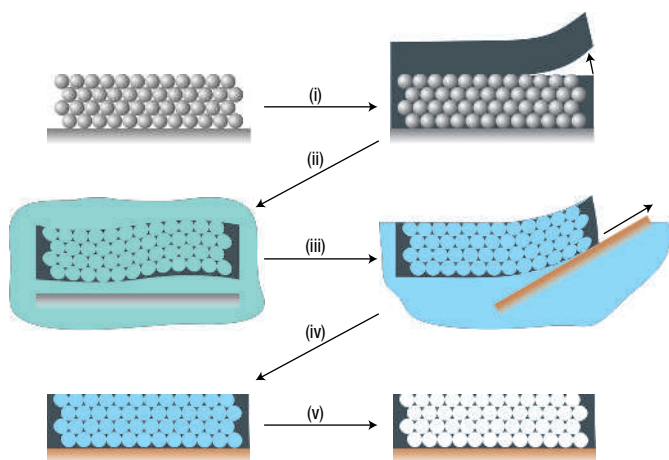
179

Figure 1 Steps in the fabrication of EPC films. (i) An interconnected SiO₂ microsphere film, with sphere diameters of 300–900 nm, on glass is infiltrated with a mixture of alkylmethacrylate and ethylene glycol diacrylate, and photopolymerized using an ultraviolet photoinitiator. After polymerization, the excess polymer is peeled off the top of the opal. (ii) The silica microspheres and the underlying substrate are dissolved in aqueous HF. (iii) The free-standing film is transferred onto the surface of distilled water. (iv) The macroporous film is transferred onto a substrate of choice. (v) The water in the voids is removed by drying in a stream of nitrogen.

peeled off, after which both the spheres and substrate are etched in dilute hydrofluoric acid. Once transferred onto a water surface, the films can be deposited onto any substrate drawn through the interface and dried to remove the water filling the periodic voids. We have used a variety of alkyl methacrylates, alkyl acrylates and mixtures thereof to fabricate robust large-area (several cm²) EPC films of variable stiffness on flat or curved glass, metal and polymer substrates.

EPC films show highly reversible structural and optical responses to compressive forces. Inspiring pioneering studies on mechanochromic PCs have been reported[8,11–13,22,23], where studies on the deformation of non-close-packed spheres embedded in hydrogel or elastomer matrices were carried out. All of these studies deal with non-porous solid materials, where a compression along one direction must be accompanied by an expansion along perpendicular directions to maintain a constant volume (Poisson ratio ~0.5). Porous polymers, on the other hand, can be compressed with a minimal expansion in other directions (Poisson ratio of near zero), reducing the redistribution of stress along lateral directions when compressed by a patterned surface. In Fig. 2a, a series of scanning electron microscopy (SEM) images is shown illustrating the effect of compression on the lattice constant in the [111] crystallographic direction (perpendicular to the substrate). It is especially noteworthy that for PCs with void sizes of about 345 nm, the [111] spacing monotonically decreases from 276 to 188 nm, whereas the dimensions within the {111} planes stay constant within experimental error. EPC compression proceeds by a reduction of the air volume fraction and the distortion of the cross-sectional void spaces from roughly circular to elliptical shape. By compressing with a patterned elastomeric stamp, it was found that feature sizes down to 5 μm could be visualized using an EPC film.

The response of EPCs to compression was evaluated using a specially designed optical setup (see Supplementary Information, Fig. S1), collecting visible-NIR reflectance spectra while applying pressure with a computerized spring-coupled microactuator. The

films have a face-centred-cubic crystal structure and show a prominent stop-gap owing to diffraction from {111} crystal planes. Compression in the [111] direction is therefore manifested as a blue-shift in the stop-gap position. In Fig. 2b the reflected stop-band position of an EPC film with 350-nm void size is plotted for a series of 30 compression–decompression cycles with an applied compressive pressure of approximately 15 kPa. An increase in pressure gradually blue-shifts the peak position by 60 nm, decreases the reflection intensity by 3% and increases the peak width by 17%. Releasing the applied pressure returns the position, intensity and width to their original positions. It can be appreciated that the deformation is highly reversible and stable to extended cycling. In Fig. 2c and d, reflectance spectra clearly show the blue-shift from visible and infrared stop-bands, respectively, on compression. It seems that an EPC film can be subjected to thousands of compression cycles without significant loss in optical quality.

The ability to optically monitor EPC compression has profound ramifications in the study of elasticity at the nanometre scale[24] where surface effects become increasingly important, and could enable the application of commercial elastomers in nanotechnology. This system provides a synthetic entry for the observation of nonlinear size-scaling behaviour, where increased surface effects are expected to become dominant in deviations from ideal elastic properties[25]. Preliminary investigations have found strong nonlinear dependence of EPC elasticity on the template sphere size, a behaviour we are actively investigating. Their regular porosity make EPCs nearly ideal candidates for optically monitored mechanical deformations using a cellular solid structural model[26], with the periodicity and volume fraction being strictly controlled by straightforward modifications of the microsphere template.

A technologically relevant application of compressively active PCs is the development of a new generation of biometric recognition devices. The most important biometric identifier is the fingerprint, with revenues from fingerprinting technologies expected to grow from $198 million in 2003 to $1.5 billion in 2008 (see http://www.biometricgroup.com). Using EPCs, we have demonstrated the first example of a high-accuracy, multichannel, time- and pressure-dependent PC colour-fingerprinting device. The dynamic behaviour of a backlit EPC film in response to compression by an index finger can be seen on video (Supplementary Information, Videos S1 and S2), and still images (Fig. 3a). Videos are captured at 29 frames per second, enabling the analysis of 174 separate images over a 6 s press–release interval. Each individual frame is specific for a particular applied pressure or relaxation time. Colour filters can be applied to generate several greyscale composites for each colour frame (Fig. 3b and Supplementary Information, Fig. S2): the resulting data show not only the characteristic line ridges, but also the pressure distributions over the finger surface. This attribute allows us to easily differentiate between an imprint from a real finger and a rubber replica (PDMS), where the latter gives much sharper pressure contrast between ridges and valleys (data not shown). A practical high-sensitivity identification device would consist of an EPC film integrated with a pressure sensor and a camera capturing images at a particular imprint pressure. Further information can be extracted from a microscopic analysis of the fingerprint pattern (Fig. 2c,d). Here, a complete visible reflectance scan was collected for each pixel and the integrated intensity for different spectral ranges could be plotted. Such selected energy fingerprint maps can facilitate data analysis by considering points above a certain intensity threshold or identify specific marks such as high- or low-intensity features.

Several other applications can be accessed through our EPC material, with its hollow voids allowing functional species to
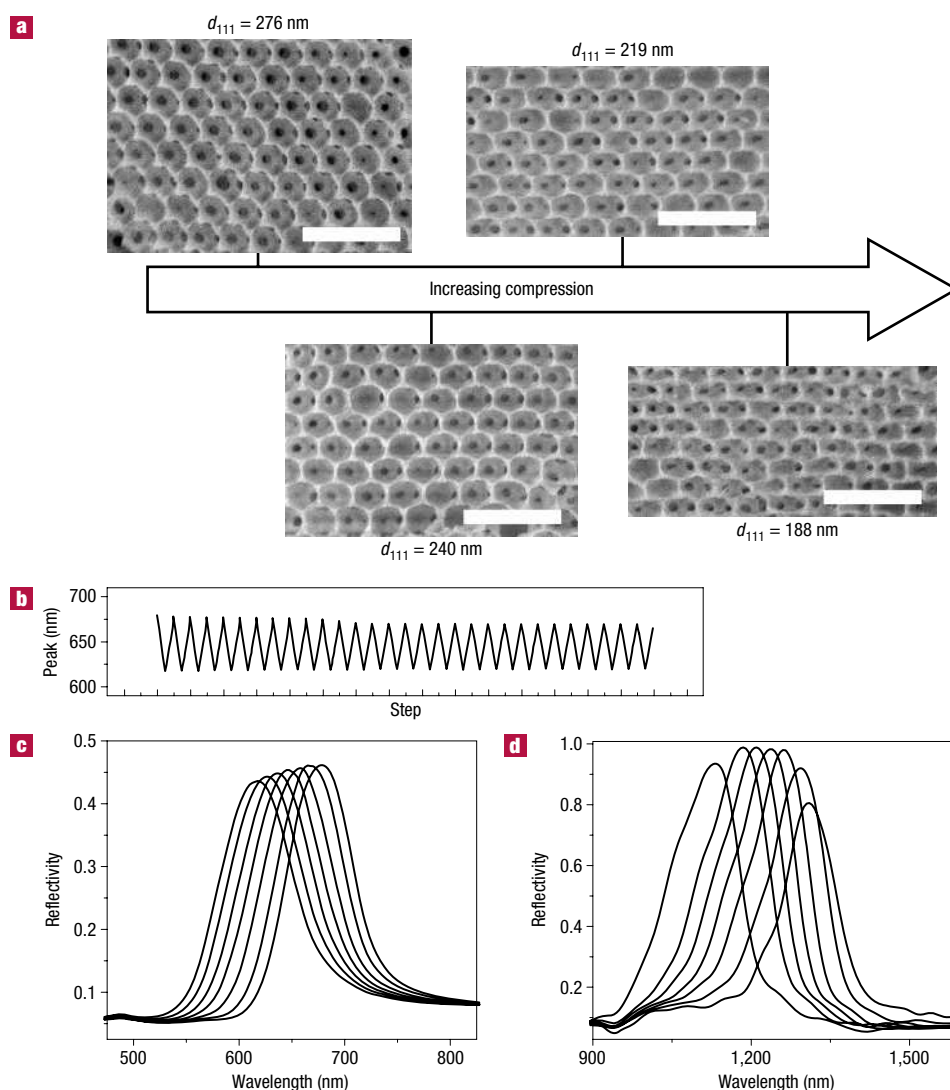
Figure 2 Mechanical and optical response of EPC films to compressive pressure. a, SEM images taken at gradually increasing compression, showing the decrease in d_{111} lattice spacing. All scale bars represent 1 μm. **b,** The compression–decompression cycling of the stop-band peak position for a 350 nm void EPC film, subjected to a spring-coupled actuator compression of 12 mm resulting in approximately 15-kPa compressive stress. Spectra were collected at 1.2-mm intervals. **c,d,** Normal incidence reflectivity spectra showing the blue-shift in the stop-band on compression of 350-nm and 710-nm void EPC samples, respectively.

be incorporated easily after fabrication. To demonstrate such a capability, we have incorporated NIR-emitting colloidal PbS quantum dots onto the surface of the polymer defining the void spaces of an EPC material. The dynamic tuning of spontaneous emission behaviour of lead chalcogenide NIR-emitting quantum dots could have profound repercussions in the development of tunable NIR light sources and high-efficiency solar cells[27]. When the stop-gap of the EPC overlaps with the PbS PL peak, the shape of the spontaneous emission curve is strongly modified, an effect that can be dynamically adjusted by compression (Fig. 4a). A similar effect has been observed in samples where rhodamine dye-modified microspheres were self-assembled in deionized media and subsequently fixed in an elastomeric matrix by photopolymerization[28]. To obtain a reference spectrum, we compress the EPC until the photonic stop-gap is blue-shifted out of the range of the PL peak. This peak represents exactly the same population of dots without the influence of the photonic band

structure. Figure 4b shows the overlap of all the collected PL spectra (normal incidence) of the same spot on the sample ($\sim$0.5 mm^2) at different applied pressures, with clearly observable suppression and enhancement relative to the reference. To quantify this effect, the PL plots are divided by the reference PL emission (Fig. 4c) to give intensity ratios[29]. Here, values above 1 represent enhancement, whereas those below 1 represent suppression. The luminescence spectra are not corrected in any way and all spectra are collected from the same spatial region of the sample, making the intensities of all curves directly comparable. The suppression follows the shift of the stop-gap and stays constant at about 60%. The enhancement is greatest at the red edge of the PL peak and reaches a maximum of about 100%.

A hallmark feature of PCs is the redistribution of photonic density of states (PDOS), which can lead to enhanced decay rates for increased PDOS and suppressed rates for decreased PDOS, as well as a pronounced direction dependence of light emission
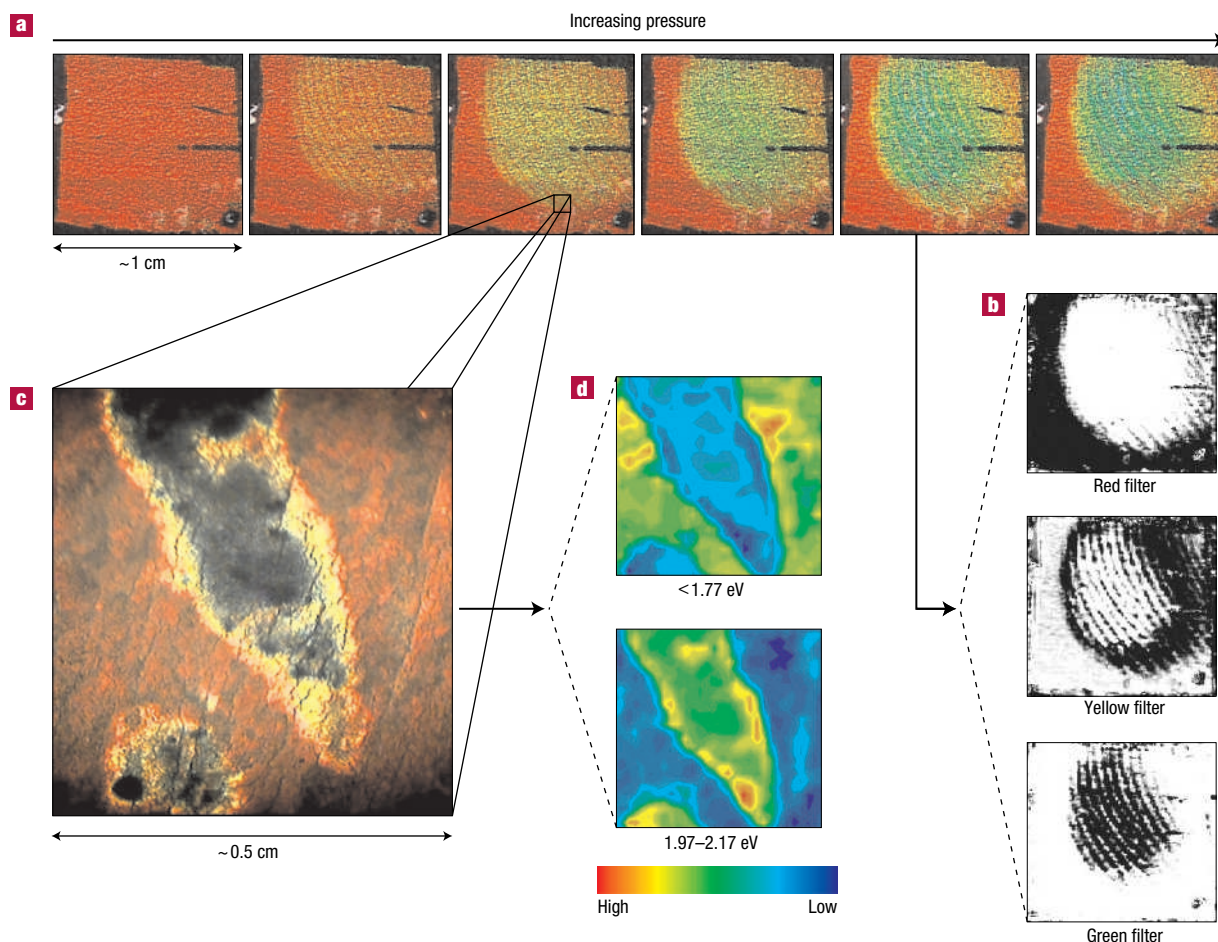
Figure 3 PC fingerprinting using EPC films. a, Still images taken during the compression of an EPC film by an index finger. **b**, Greyscale images of one of the frames in **a**, obtained after the application of colour filters. The black regions in each filtered image correspond to the distribution of a particular pressure range, increasing from red to green. **c**, A microscope image of a single line termination in a fingerprint-compressed EPC. A complete reflection spectrum has been collected for each pixel in this image. **d**, Energy mapping of the spectral data collected by microspectroscopy, where red is the highest intensity and blue the lowest. The top frame shows the integrated intensity in the energy range of less than 1.77 eV, whereas the bottom frame shows the integrated intensity in the range 1.97–2.17 eV.

and propagation. To further investigate the effect of the EPC on the quantum-dot emission, PL lifetime experiments were carried out. In Fig. 4e we show PL lifetime data for a sample with and without compression along the ⟨111⟩ direction, with the corresponding normal-incidence stop-bands shown in Fig. 4d, overlaid onto the PL spectrum of the same quantum dots dried on a glass slide. The luminescence decay curves are typical of dried quantum dots, as they show the effects of energy-transfer processes between dots of different sizes[30]. The initial fast decay is non-exponential and comparable in both curves, dominated by energy-transfer processes that should not be significantly altered by a modification of the PDOS. The slower component (after 1.5 μs), which is nearly exponential, is the most affected as it is almost entirely governed by radiative recombination. When the pseudogap lays on top of the luminescence curve (black curve, Fig. 4e), the luminescence decay after 1.5 μs is 1.47 ± 0.05 μs, significantly slower than in the case of the pseudogap being blue-shifted with respect to the luminescence (grey curve), where the decay is 1.27 ± 0.03 μs. The magnitude of the changes in lifetime, $16 \pm 4\%$, is significant when one considers the combined effects of the low refractive index contrast in the material and relatively thin

samples. In other studies[31,32], direction-dependent enhancement and suppression of luminescence was observed with changes in luminescence lifetimes of about 5%. A strong modulation in luminescence lifetimes[3,4] requires a strongly scattering system and a crystal with a much greater number of unit cells in the (111) direction. The magnitude of the luminescence lifetime change is in qualitative agreement with theoretical simulations of the local PDOS in these EPC samples (finite-difference time domain calculations, results not shown), although these values are very sensitive to the precise locations of the quantum dots in the EPC scaffold considering the anisotropic nature of the deformation. This reversible tuning of the luminescence profile and lifetime from quantum dots is unprecedented and worthy of further investigation, especially considering the vast number of possible applications of NIR-emitting quantum dots.

We expect tunable porous EPCs will be applicable to several emerging applications such as new fingerprinting materials, piezo-electric driven colour displays, accelerometer sensors for air-bag release in automobiles, sensors to monitor explosion shockwaves, colour sensing of strain in high-rise buildings, as well as tunable band-edge LEDs and laser sources.
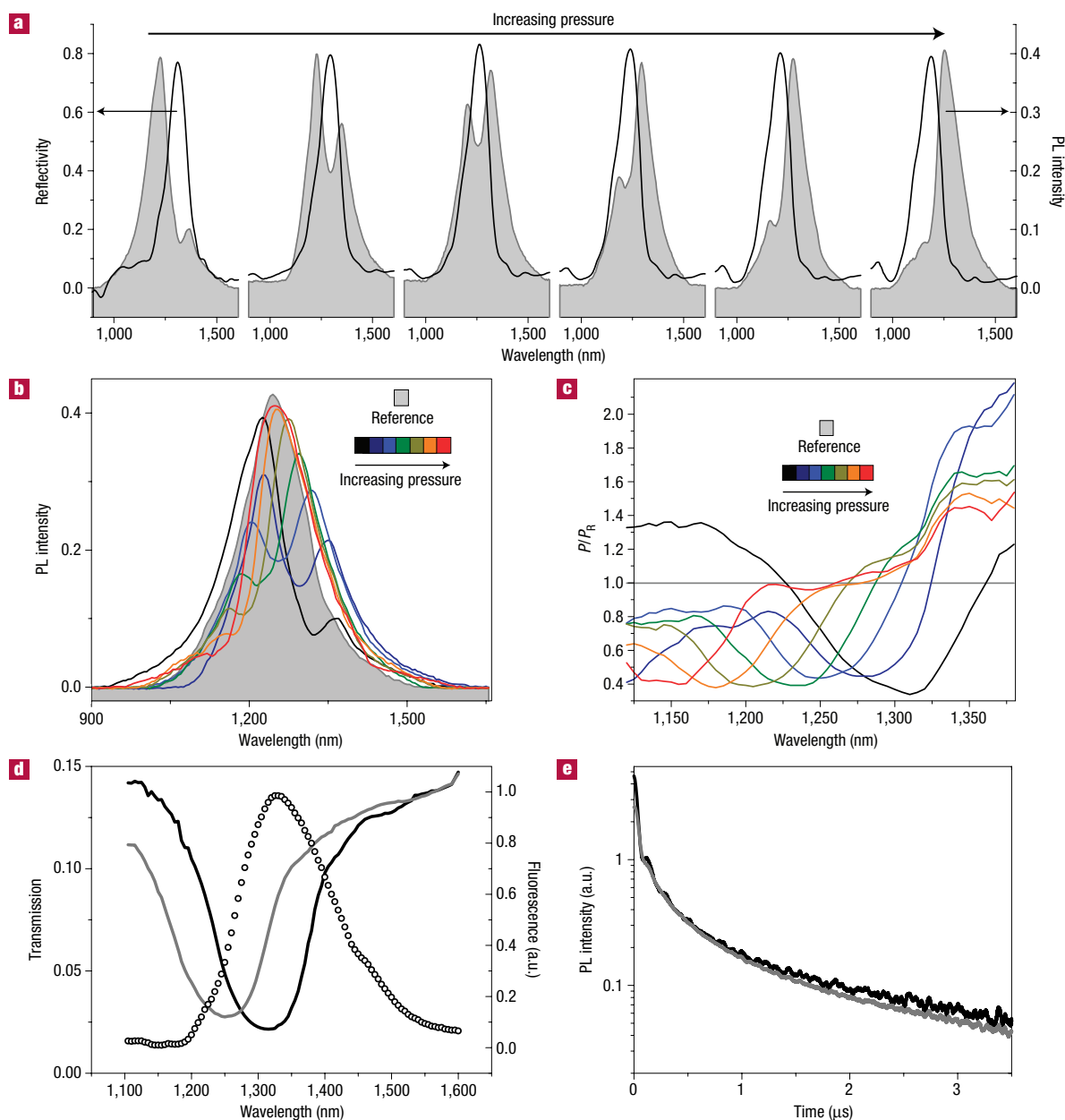
Figure 4 Tuning of NIR PL properties from quantum dots incorporated into EPCs. a, Overlay of the EPC stop-band (solid black line) and the PbS PL peak (grey filled curve), for increasing degrees of compression. **b,** Overlay of all collected PL curves over one compression cycle, with the grey curve representing the PbS PL with no influence from the stop-gap. **c,** Intensity ratio of the PL curves in **b** relative to the reference. P/P_R represents the photoluminescence intensity of the sample divided by that of the reference. Values above 1 represent enhancement in PL, values below 1 represent suppression. **d,** Graph showing the transmission spectra of an EPC sample in its native (black solid curve) and compressed (grey solid curve) states. Overlayed onto this is the PL spectrum of PbS quantum dots dried on a glass slide, obtained on excitation of the dots with a high (82 MHz) repetition rate (Ti:sapphire) mode-locked laser operated at 810 nm. **e,** Luminescence decay curves for quantum dots infiltrated into an EPC sample, in both the native (black solid curve) and compressed (grey solid curve) states.

METHODS

All chemicals were purchased from Aldrich unless otherwise specified.

TEMPLATE FABRICATION

Silica microspheres were synthesized according to a modified Stöber process[33]. Colloidal crystal films were generated using evaporation-induced self-assembly either at room temperature[20] for spheres below 400 nm or under isoconvective heating conditions[21] for spheres above 400 nm, on glass microscope slides

(Fisher). After deposition, films were mechanically stabilized by overnight treatment in tetramethoxysilane vapour.

POLYMER SYNTHESIS

In a typical experiment, ethylene glycol dimethacrylate crosslinker (0.800 g, 4.04 mmol) was added to neat ethylhexyl methacrylate (8.00 g, 40.3 mmol) at 20 °C in the absence of light. Volatiles were removed *in vacuo* for 5 min and phenylbis(2,4,6-trimethylbenzoyl)phosphine oxide initiator (0.080 g,

0.191 mmol) was added at 20 °C and stirred under nitrogen for 10 min. The resultant yellow solution was transferred to a vial containing the colloidal crystal template, to completely cover the template. The vial was cooled to 5 °C and photo-irradiated for 5 h using a 125 W high-pressure Hg arc lamp with a pyrex-glass filter (wavelength $\lambda \gtrsim 300$ nm) to give a template-embedded piece of colourless solid elastomer. Synthesis of other polymer compositions was performed according to this procedure, replacing ethylhexyl methacrylate with lauryl methacrylate, butyl methacrylate, methyl methacrylate, butyl acrylate, hexyl acrylate or mixtures thereof.

EPC SYNTHESIS

The glass vial was cracked open and excess elastomer was slowly peeled off the surface of the template. The polymer–silica composite film was then sectioned into pieces of the desired size and these were immersed in 2% aqueous hydrogen fluoride. After 5–20 min, the polymer film floats off the underlying substrate and is transferred onto distilled water where it floats at the air–water interface. After standing for 10 min, the floating film is deposited onto a given flat or curved substrate by withdrawing this substrate through the air–water interface. Excess water is soaked with tissue paper, and the water in the voids of the structure is evaporated under a stream of nitrogen gas to give the EPC film.

SEM

SEM measurements were performed on a Hitachi S-5200 SEM, using an accelerating voltage of 1.5 kV and arc-coating the samples with a thin carbon film before imaging. The monomer composition of the imaged samples was a methyl methacrylate–butyl methacrylate mixture, which is glassy at room temperature. The EPC was heated to between 60 °C and 120 °C, compressed, then cooled to freeze-in the compression. Samples were then cleaved and imaged as cross-sections.

OPTICAL PRESSURE CYCLING

The EPCs were reversibly compressed and decompressed using a computer-controlled microactuator. The samples were illuminated with a 60 W tungsten–halogen lamp, where the reflected light was dispersed in a 0.25 m scanning monochromator and detected with a thermo-electrically cooled extended InGaAs detector for each compression step.

NIR EMISSION

Colloidal PbS quantum dots were prepared according to a high-temperature organometallic route[34]. A drop of a concentrated solution in hexane was dropped onto an EPC film and rapidly dried with a stream of nitrogen. The quantum dots were excited with 0.75 mW continuous wave output of a frequency-doubled Nd:YAG laser at 532 nm. PL was measured with the same setup as the reflectance spectra.

LUMINESCENCE LIFETIME EXPERIMENTS

Quantum dots infiltrated into the EPC samples were excited with <4 mJ, 10 ns pulses using a Nd:Yag Q-switch laser operated at 1,064 nm. Every curve is averaged over 512 pulses to reduce experimental noise. The fluorescence was collected by an InGaAs photodiode, which was sufficiently fast (20 ns raise time) to resolve the time decay. The excitation was performed at oblique incidence, 60° from the [111] direction, whereas the fluorescence was collected with a 50 mm lens with a 30° focal cone. The residual excitation light was blocked with frequency selective filters, with a suppression ratio of 10^{-6}. The fluorescence decay was monitored as a function of the pressure applied to the PCs in the [111] direction, normal to the supporting substrate surface.

References

1. Lopez, C. Materials aspects of photonic crystals. *Adv. Mater.* **15,** 1679–1704 (2003).
2. Joannopoulos, J. D., Villeneuve, P. R. & Fan, S. H. Photonic crystals: Putting a new twist on light. *Nature* **386,** 143–149 (1997).
3. Ogawa, S. P., Imada, M., Yoshimoto, S., Okano, M. & Noda, S. Control of light emission by 3D photonic crystals. *Science* **305,** 227–229 (2004).
4. Lodahl, P. *et al.* Controlling the dynamics of spontaneous emission from quantum dots by photonic crystals. *Nature* **430,** 654–657 (2004).
5. Vlasov, Y. A., Luterova, K., Pelant, I., Honerlage, B. & Astratov, V. N. Enhancement of optical gain of semiconductors embedded in three-dimensional photonic crystals. *Appl. Phys. Lett.* **71,** 1616–1618 (1997).
6. Yoshino, K. *et al.* Observation of inhibited spontaneous emission and stimulated emission of rhodamine 6G in polymer replica of synthetic opal. *Appl. Phys. Lett.* **73,** 3506–3508 (1998).
7. Painter, O. *et al.* Two-dimensional photonic band-gap defect mode laser. *Science* **284,** 1819–1821 (1999).
8. Holtz, J. H. & Asher, S. A. Polymerized colloidal crystal hydrogel films as intelligent chemical sensing materials. *Nature* **389,** 829–832 (1997).
9. Li, Y. Y. *et al.* Polymer replicas of photonic porous silicon for sensing and drug delivery applications. *Science* **299,** 2045–2047 (2003).
10. Arsenault, A. C., Miguez, H., Kitaev, V., Ozin, G. A. & Manners, I. A polychromic, fast response metallopolymer gel photonic crystal with solvent and redox tunability: A step towards photonic ink (P-Ink). *Adv. Mater.* **15,** 503–507 (2003).
11. Foulger, S. H. *et al.* Photonic bandgap composites. *Adv. Mater.* **13,** 1898–1901 (2001).
12. Foulger, S. H. *et al.* Photonic crystal composites with reversible high-frequency stop band shifts. *Adv. Mater.* **15,** 685–689 (2003).
13. Haacke, G., Panzer, H. P., Magliocco, L. G. & Asher, S. A. US patents 5,266,238, and 5,368,781 (1993).
14. Li, Y. Y. *et al.* Polymer replicas of photonic porous silicon for sensing and drug delivery applications. *Science* **299,** 2045–2047 (2003).
15. Yablonovitch, E. Inhibited spontaneous emission in solid-state physics and electronics. *Phys. Rev. Lett.* **58,** 2059–2062 (1987).
16. John, S. Strong localization of photons in certain disordered dielectric superlattices. *Phys. Rev. Lett.* **58,** 2486–2489 (1987).
17. Blanco, A. *et al.* Large-scale synthesis of a silicon photonic crystal with a complete three-dimensional bandgap near 1.5 micrometres. *Nature* **405,** 437–440 (2000).
18. Noda, S., Tomoda, K., Yamamoto, N. & Chutinan, A. Full three-dimensional photonic bandgap crystals at near-infrared wavelengths. *Science* **289,** 604–606 (2000).
19. Nishimura, S. *et al.* Standing wave enhancement of red absorbance and photocurrent in dye-sensitized titanium dioxide photoelectrodes coupled to photonic crystals. *J. Am. Chem. Soc.* **125,** 6306–6310 (2003).
20. Jiang, P., Bertone, J. F., Hwang, K. S. & Colvin, V. L. Single-crystal colloidal multilayers of controlled thickness. *Chem. Mater.* **11,** 2132–2140 (1999).
21. Wong, S., Kitaev, V. & Ozin, G. A. Colloidal crystal films: Advances in universality and perfection. *J. Am. Chem. Soc.* **125,** 15589–15598 (2003).
22. Asher, S. A., Holtz, J., Liu, L. & Wu, Z. J. Self-assembly motif for creating submicron periodic materials—polymerized crystalline colloidal arrays. *J. Am. Chem. Soc.* **116,** 4997–4998 (1994).
23. Jethmalani, J. M. & Ford, W. T. Diffraction of visible light by ordered monodisperse silica-poly(methyl acrylate) composite films. *Chem. Mater.* **8,** 2138–2146 (1996).
24. Wong, E. W., Sheehan, P. E. & Lieber, C. M. Nanobeam mechanics: Elasticity, strength, and toughness of nanorods and nanotubes. *Science* **277,** 1971–1975 (1997).
25. Miller, R. E. & Shenoy, V. B. Size-dependent elastic properties of nanosized structural elements. *Nanotechnology* **11,** 139–147 (2000).
26. Gibson, L. J. Cellular solids. *Mater. Res. Soc. Bull.* **2,** 270–271 (2003).
27. Ellingson, R. J. *et al.* Highly efficient multiple exciton generation in colloidal PbSe and PbS quantum dots. *Nano Lett.* **5,** 865–871 (2005).
28. Lawrence, J. R. *et al.* Dynamic tuning of photoluminescent dyes in crystalline colloidal arrays. *Adv. Mater.* **17,** 2344–2349 (2005).
29. Koenderink, A. F., Bechger, L., Schriemer, H. P., Lagendijk, A. & Vos, W. L. Broadband fivefold reduction of vacuum fluctuations probed by dyes in photonic crystals. *Phys. Rev. Lett.* **88,** 143903 (2002).
30. Crooker, S. A., Hollingsworth, J. A., Tretiak, S. & Klimov, V. I. Spectrally resolved dynamics of energy transfer in quantum-dot assemblies: Towards engineered energy flows in artificial materials. *Phys. Rev. Lett.* **89,** 186802 (2002).
31. Barth, M., Gruber, A. & Cichos, F. Spectral and angular redistribution of photoluminescence near a photonic stop band. *Phys. Rev. B* **72,** 085129 (2005).
32. Viasnoff-Schwoob, E. *et al.* Spontaneous emission enhancement of quantum dots in a photonic crystal wire. *Phys. Rev. Lett.* **95,** 183901 (2005).
33. Stöber, W., Fink, A. & Bohn, E. Controlled growth of monodisperse silica spheres in micron size range. *J. Colloid Interface Sci.* **26,** 62–69 (1968).
34. Cademartiri, L. *et al.* Nanocrystals as precursors to flexible functional films. *Small* **1,** 1184–1187 (2005).